Inorganic Chemistry

Article

pubs.acs.org/IC

Synthesis, Characterization, MCD Spectroscopy, and TD-DFT Calculations of Copper-Metalated Nonperipherally Substituted Octaoctyl Derivatives of Tetrabenzotriazaporphyrin, *cis*- and *trans*-Tetrabenzodiazaporphyrin, Tetrabenzomonoazaporphyrin, and Tetrabenzoporphyrin

John Mack,[†,‡] Lydia Sosa-Vargas,[§] Simon J. Coles,[⊥] Graham J. Tizzard,[⊥] Isabelle Chambrier,[§] Andrew N. Cammidge,*[,§] Michael J. Cook,*[,§] and Nagao Kobayashi*[,‡]

[‡]Department of Chemistry, Graduate School of Science, Tohoku University, Sendai 980-8578, Japan

[§]School of Chemistry, University of East Anglia, Norwich NR4 7TJ, U.K.

[⊥]EPSRC National Crystallography Service, School of Chemistry, University of Southampton, Southampton SO17 1BJ, U.K.

ABSTRACT: Synthesis of the title compounds has been achieved through refinement of a recently reported synthetic protocol whereby varying equivalents of MeMgBr are reacted with 1,4-dioctylphthalonitrile to produce mixtures favoring specific hybrid structures. The initially formed magnesium-metalated compounds are obtained as pure materials and include, for the first time, both isomers (cis and trans) of tetrabenzodiazaporphyrin. The compounds were demetalated to the metal-free analogues, which were then converted into the copper-metalated derivatives. The X-ray structure of the copper tetrabenzotriazaporphyrin derivative is reported. The metal-free and copper-metalated macrocycles exhibit columnar mesophase behavior, and it is found that the mesophase stability is unexpectedly reduced in the diazaporphyrin derivatives compared to the rest of the series. The results of time-dependent density functional theory calculations for the copper complexes are compared to the observed optical properties. Michl's perimeter model was used as a conceptual framework for analyzing the magnetic circular dichroism spectral data, which predicted and accounted for trends in the observed experimental spectra.

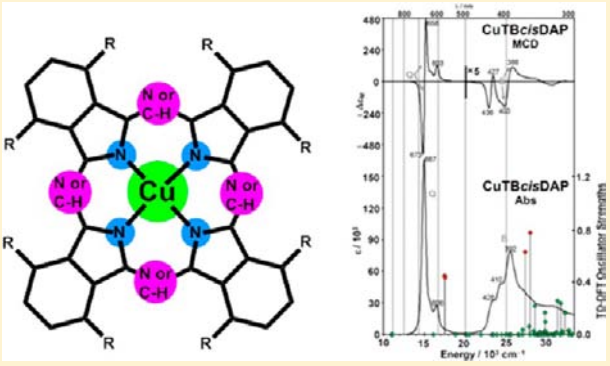

INTRODUCTION

Tetrabenzotriazaporphyrins (TBTrAPs), *cis*- and *trans*-tetrabenzodiazaporphyrins (TB*cis*DAP and TB*trans*DAP), and tetrabenzomonoazaporphyrins (TBMAPs) (Figure 1) can be regarded as hybrid structures of the phthalocyanine (Pc) and tetrabenzoporphyrin (TBP) macrocycles. They differ from these two structural types through the presence of a combination of both aza and methine groups within the core heterocyclic component, i.e., the unit that gives rise to the cyclic 18π-electron system. Unlike TBPs and, in particular, Pc's, the hybrid structures have been relatively little studied. Kobayashi's review of the literature of the hybrid macrocycles prior to 2002 indicated that about 50 examples had been reported, a number of which were differently metalated examples of the same ligand.[1] Although there has been an increasing interest in these compounds, a review of the literature to early 2011 by the Norwich group[2] showed that the number of published papers and patents concerning these compounds was still no more than 100. A plausible reason for this may lie in the synthetic challenge inherent in the selective incorporation of specified combinations of the aza and methine groups.

Early syntheses of hybrid compounds undertaken independently by Heilberger and von Rebay,[3] Dent,[4] and Linstead et al.[5] in the 1930s utilized reactions of phthalonitrile with methylmagnesium iodide, methyllithium, or phthalimidine-acetic acid. These provided the first examples of unsubstituted metalated TBTrAPs and TBMAPs. Much more recent work, in particular by the groups of Galanin et al.,[6] Leznoff et al.,[7] Luk'yanets et al.,[8] and others,[9] extended both the chemistry and range of derivatives available, leading to the synthesis of examples of all four hybrid compounds. In particular, attention has been given to the incorporation of substituents on the benzenoid rings and/or at the *meso*-carbon atoms.[2]

Recently, the Norwich group reported an unexpectedly facile access to nonperipherally substituted octahexyl and octadecyl derivatives of three of the possible four hybrid compounds, viz., TBTrAP, TB*cis*DAP, and TBMAP, as well as TBP.[10] The compounds were generally obtained as mixtures by merely reacting 3,6-dialkylphthalonitrile with varying equivalents of

Received: August 3, 2012
Published: November 9, 2012

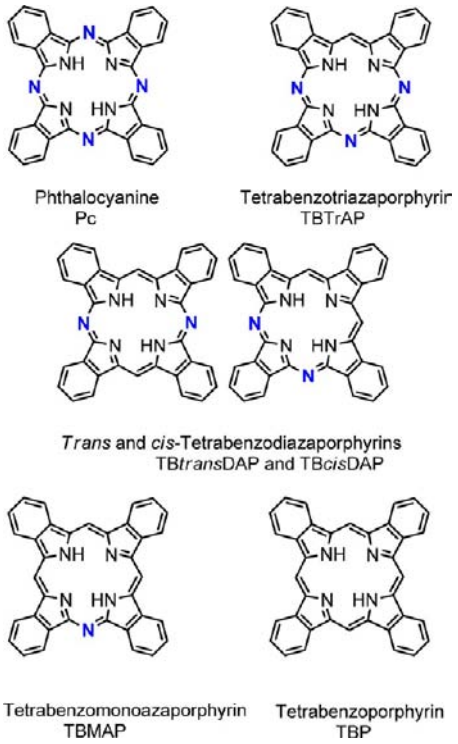

Figure 1. Molecular structures showing the relationship of the unmetalated macrocycles Pc, TBTrAP, TB*cis*DAP, TB*trans*DAP, TBMAP, and TBP.

methylmagnesium bromide (MeMgBr), with higher equivalents of the latter leading to greater preponderances of the more methine-containing derivatives. Individual compounds were isolated in modest yields.

In the present work, we have sought to optimize the reaction conditions for generating the hybrid structures using 3,6-dioctylphthalonitrile as the precursor. In this case, the isolated products have included the TB*trans*DAP derivative for the first time alongside the three other hybrid derivatives and the TBP analogue; this study therefore reports a comparison of the first full series of substituted, single-isomer hybrids. The compounds, isolated as the magnesium-metalated derivatives, were each demetalated and then reacted with copper acetate to form the copper-metalated compounds. The X-ray structure of the copper-metalated TBTrAP is reported. The liquid-crystal properties of all of the metal-free and copper derivatives have been investigated and compared. Magnetic circular dichroism (MCD) spectra of the copper-metalated macrocycles and time-dependent density functional theory (TD-DFT) calculations are reported for the unsubstituted copper-metalated ligands. Michl's perimeter model[11] is used as a conceptual framework to analyze the results.

RESULTS AND DISCUSSION

Preparation and Characterization of Compounds. The general scheme used to prepare the novel octaoctyl-substituted hybrid compounds is shown in Figure 2 and was applied earlier to prepare the octahexyl- and octadecyl-substituted macrocycles referred to above.[10] The route is based broadly upon the early procedure used by Linstead and Barrett for obtaining the unsubstituted macrocycles.[5] As shown in Figure 2, the macrocyclic ligands are obtained over two steps that involve a change of the solvent. The products are isolated initially as the magnesium-metalated derivatives.

In the present work, preliminary studies using varying equivalents of MeMgBr to 1 equiv of 3,6-dioctylphthalonitrile provided for the first time samples of all four magnesium-

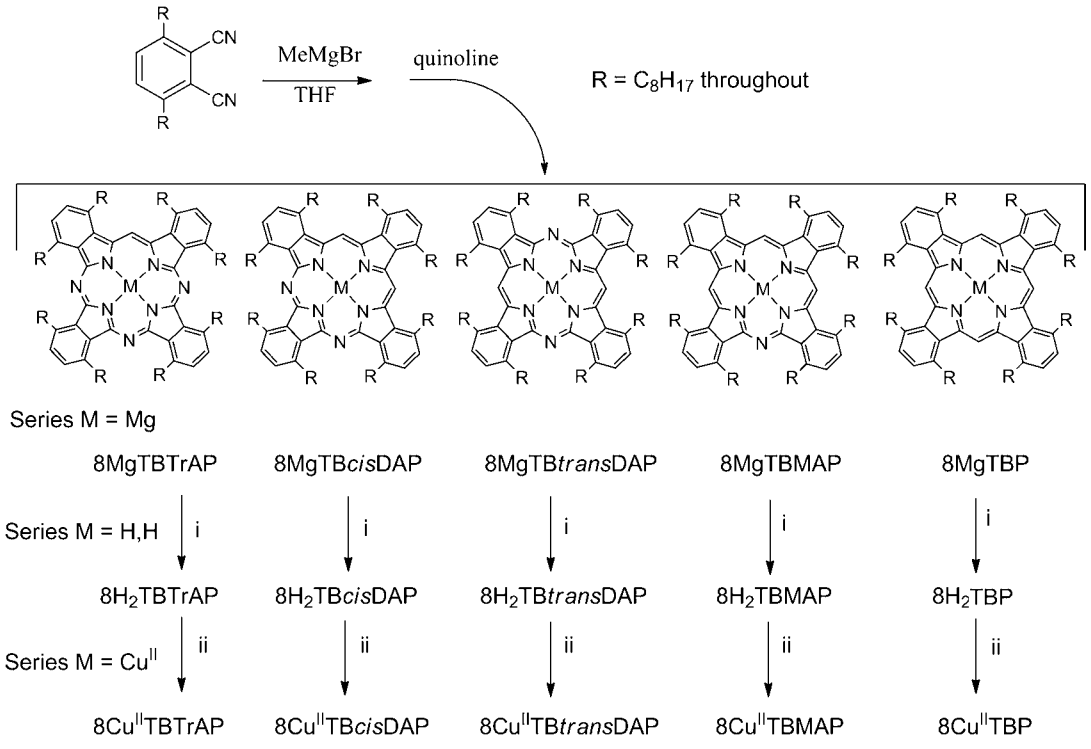

Figure 2. Synthetic scheme and notation used for the compounds reported in the paper. Eight as a prefix to each notation signifies that the chain length of each alkyl group contains eight carbon atoms. Reagents: (i) acetic acid; (ii) copper acetate.

dx.doi.org/10.1021/ic301712h | *Inorg. Chem.* 2012, 51, 12820−12833

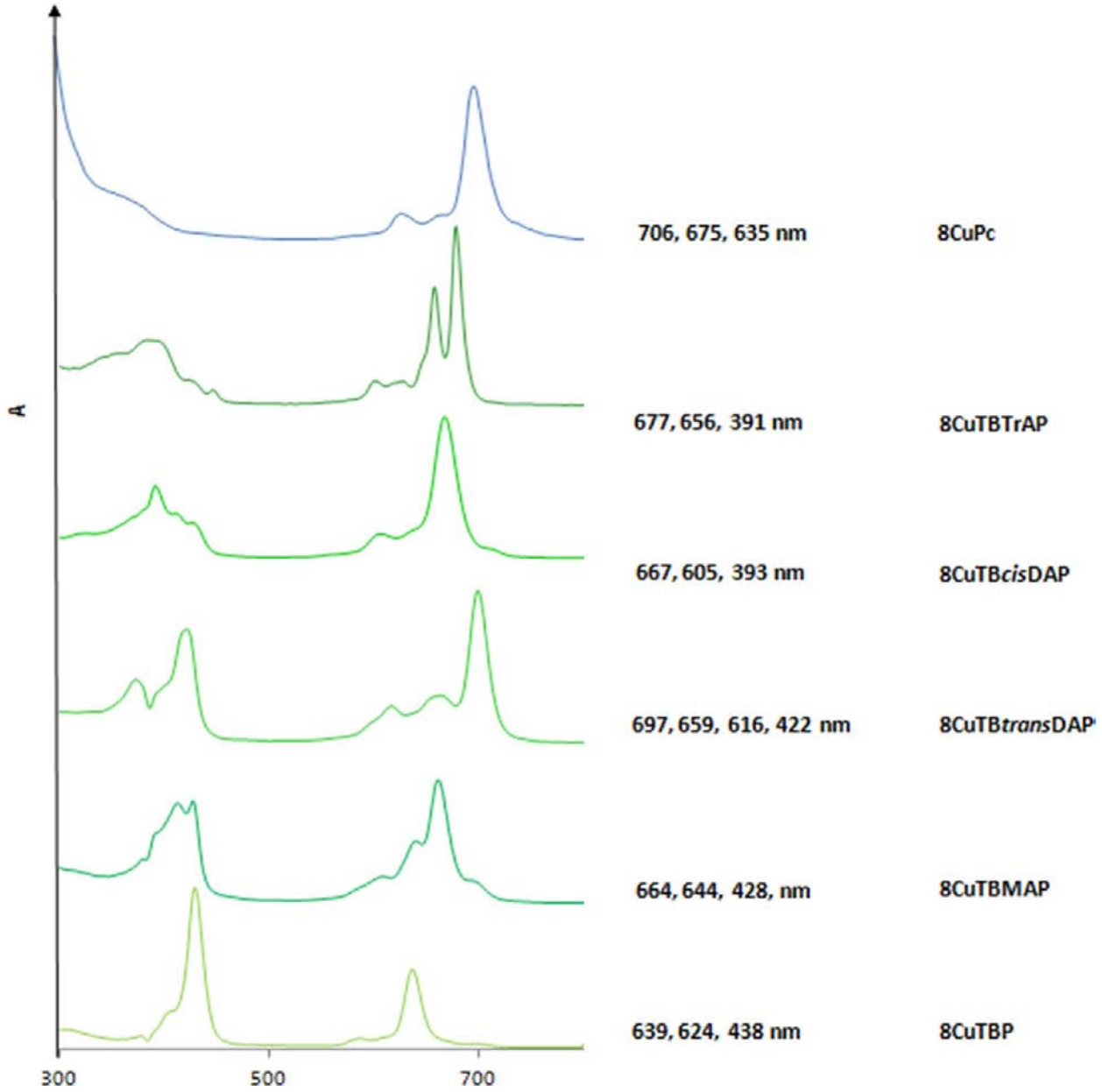

Figure 3. UV/vis absorption spectra of the copper-metalated macrocycles showing λ_{max} for the main spectral bands. As the number of aza nitrogen atoms increases, the B band shifts to the blue from 438 nm and broadens, while the Q band shifts to the red from 639 nm and steadily intensifies relative to the B band.

metalated hybrid derivatives together with TBP. These were separated chromatographically, all as viscous gums. They were identified and characterized by matrix-assisted laser desorption ionization (MALDI) time-of-flight (TOF) mass spectrometry (MS), with each compound giving a characteristic isotopic cluster for the molecular mass ion, and by ^{1}H NMR spectroscopy; in particular, the isomeric TB*cis*DAP and TB*trans*DAP compounds were readily distinguished by the signals in the aromatic and benzylic proton regions. The compounds, and those of the target copper-metalated derivatives, were further characterized by their UV/vis absorption spectra (Figure 3), which reveal, in particular, the differences in the Q band energies for the isomeric TBDAPs that are discussed later.

During this study, experiments revealed aspects of the role of the solvent and the conditions for the preparation of the compounds. With regard to the first step, the reaction of MeMgBr with 3,6-dioctylphthalonitrile in tetrahydrofuran (THF) was found to require 30 min of reflux prior to removal of the solvent. Very poor conversions followed when the first step was undertaken at room temperature even after the reaction was left to stand for over 72 h. The use of diethyl ether rather than THF as the solvent also led to a very poor yield of the final material. In the second step, it was also noted that when the second solvent, quinoline, was added at ca. 100 °C rather than at room temperature, the final yields were very erratic, sometimes high and sometimes low. A further observation concerned the state of quinoline used in the reaction. The highest yields of recovered mixtures of hybrids were obtained using freshly distilled quinoline, suggesting that oxidative decomposition pathways compete with macrocycle formation. The use of quinoline exposed to air led to

dx.doi.org/10.1021/ic301712h | *Inorg. Chem.* 2012, 51, 12820−12833

significantly reduced amounts of the hybrid materials (Table 1). All subsequent reactions were therefore carried out using freshly distilled quinoline that was then degassed with argon. The reaction was then undertaken under an argon atmosphere.

Table 1. Variation in the Aggregate Yields of the Magnesium-Metalated Macrocycles Using Quinoline as the Reaction Solvent in the Second Step When Exposed to Air over Several Days[a]

condition of quinoline	crude product (mg)	overall yield (%)
freshly distilled	87	43
after 1 day	66	33
after 2 days	29	14
after 3 days	15	7

[a]Initial amount of starting material used = 200.0 mg.

In the previous study of the synthesis of hybrid compounds obtained when MeMgBr was reacted with 3,6-dihexylphthalonitrile and 3,6-didecylphthalonitrile,[10] the yields reported were of individual magnesium-metalated macrocyclic products isolated after column chromatography. In the present work, a further series of experiments under the optimal conditions referred to above were undertaken that used ^{1}H NMR spectroscopy to more accurately monitor the composition of the crude product mixtures using the integrated intensities of the ^{1}H NMR signals characteristic of particular protons in each hybrid compound. Typically, these were the methine and aromatic protons. The weights of the recovered mixtures as a mean of two parallel experiments, each using 200 mg of 3,6-dioctylphthalonitrile and from 1 to 5 equiv of MeMgBr, are shown in Table 2. The aggregate recovered yields were a little over 50% when 2 or 3 equiv of MeMgBr was used and very low when 1 or 5 equiv was used. The table also shows the calculated percent yield of each magnesium-metalated component using different equivalents of MeMgBr. These are based on the analysis of the ^{1}H NMR signal intensities referred to above and ignoring the very minor differences in the molecular masses of the compounds. It is clear that there is no evidence for formation of the Pc derivative in any reaction. A significant amount of TBP was obtained when 3 equiv of MeMgBr was used. Indeed, the results from experiments using 2 and 3 equiv of MeMgBr show greater amounts of the more methane-rich compounds than those using 3 equiv of MeMgBr. This is in line with earlier results for the octahexyl- and octadecyl-substituted homologues. With regard to the use of 4 equiv of MeMgBr, there is no clearly favored product within this low-yield reaction.

The separated magnesium-metalated products were demetalated using acetic acid. The metal-free derivatives were satisfactorily characterized by both ^{1}H NMR spectroscopy and MALDI-TOF-MS, with each compound giving a signal for the molecular ion. Their isotope distribution patterns matched precisely with theoretical prediction, unambiguously verifying the identification (molecular formula) of each compound.

The metal-free compounds were then converted into their copper-metalated analogues by reacting them with copper acetate. The products were characterized by MALDI-TOF-MS and elemental analysis. Crystals suitable for X-ray diffraction were obtained for 8CuTBTrAP, and its structure, shown in Figure 4, reveals an essentially planar macrocyclic core, similar in conformation to the related magnesium derivative bearing eight hexyl chains.[10]

It is well-known that Pc's substituted with eight alkyl groups (of appropriate length) form discotic liquid-crystal phases, and indeed those substituted at the nonperipheral sites show a rich polymesomorphism in many cases.[12,13] We have previously reported that hybrid structures also show mesophase behavior,[10,14] and it is therefore not surprising that the present compounds show columnar liquid-crystal phases at elevated temperatures. Again we find mesophase−mesophase transitions for many derivatives (described as D1−D4 columnar phases following the original convention reported for the parent Pc's). Figure 5 shows the detailed transition temperature and phase trends for the series of copper hybrids, and it is immediately apparent that the TBDAP derivatives, in particular 8Cu^{II}TB*trans*DAP, are revealed to be anomalous within the series. The cis isomer shows a relatively narrow mesophase range with both a depressed transition into the isotropic phase and a raised melting point. In contrast, the trans-isomer transition temperatures decreased by ca. 100 °C compared to the rest of the series. These intriguing observations were not predicted and cannot be simply rationalized but imply that the packing of the macrocyclic cores in the crystal and columnar mesophase is somehow disfavored compared to the other hybrids.

MCD and the Electronic Structure of Porphyrinoids. MCD spectroscopy[15] has previously been used to definitively identify the main electronic bands of TBTrAPs and a tetranaphthotriazaporphyrin.[16] In this paper, the MCD spectral data are used to validate theoretical descriptions of the electronic structures provided by calculated TD-DFT and ZINDO/s spectra. Analysis of the MCD spectra is based on intensity mechanisms described by the Faraday $\mathcal{A}_1$, $\mathcal{B}_0$, and C_0 terms.[15] The MCD spectra of D_{4h}-symmetric porphyrinoid complexes are usually dominated by derivative-shaped Faraday $\mathcal{A}_1$ terms, when the ground state is orbitally nondegenerate, due to the Zeeman splitting of orbitally degenerate $\pi\pi^*$ excited states. When there is no 3-fold or higher axis of symmetry, the $\mathcal{A}_1$ terms are replaced by coupled pairs of oppositely signed and Gaussian-shaped Faraday $\mathcal{B}_0$ terms. Although there is sometimes scope for the temperature-dependent Kramers doublet C_0 term intensity in the MCD spectra of porphyrinoids even when the ground state is orbitally nondegenerate if S =

Table 2. Effect of the Number of Equivalents of MeMgBr Used in the Reaction on the Composition of the Product Mixture As Assessed by ^{1}H NMR Spectroscopy

8MgTBP	8MgTBMAP	8MgTB*cis*DAP	8MgTB*trans*DAP	8MgTBTrAP	equiv of MeMgBr
		trace	trace	5%	1.0
6%	7%	5%	3%	31%	2.0
21%	18%	6%	6%		3.0
3%	6%	7%	3%	6%	4.0
trace					5.0

dx.doi.org/10.1021/ic301712h | *Inorg. Chem.* 2012, 51, 12820−12833

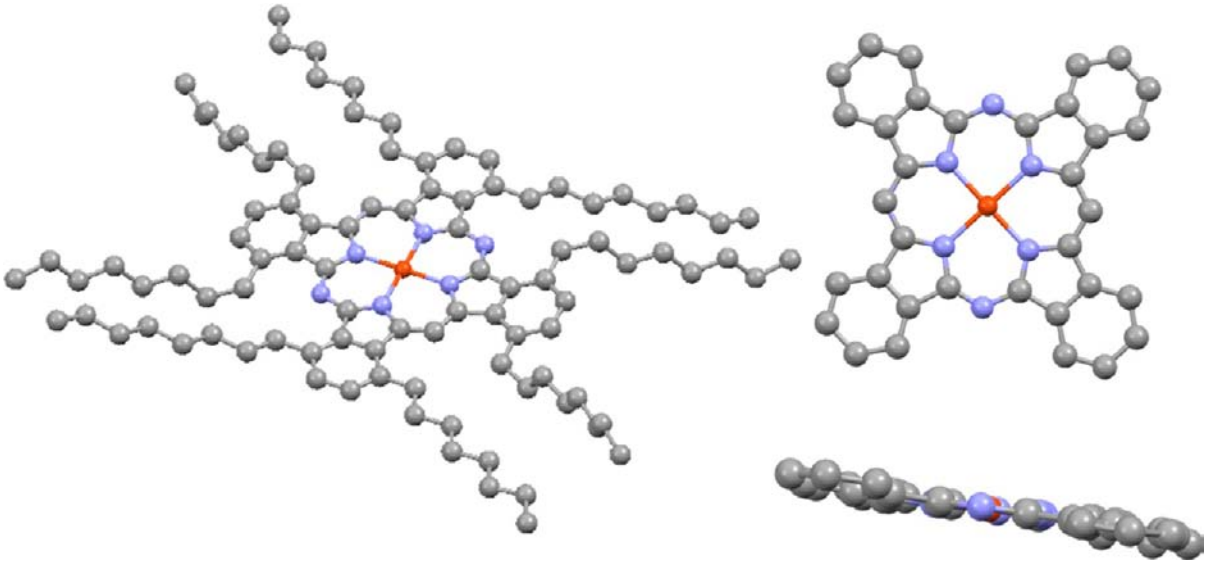

Figure 4. Crystal structure of 8Cu^{II}TBTrAP showing a near-planar core (side chains omitted for clarity on the front and side views).

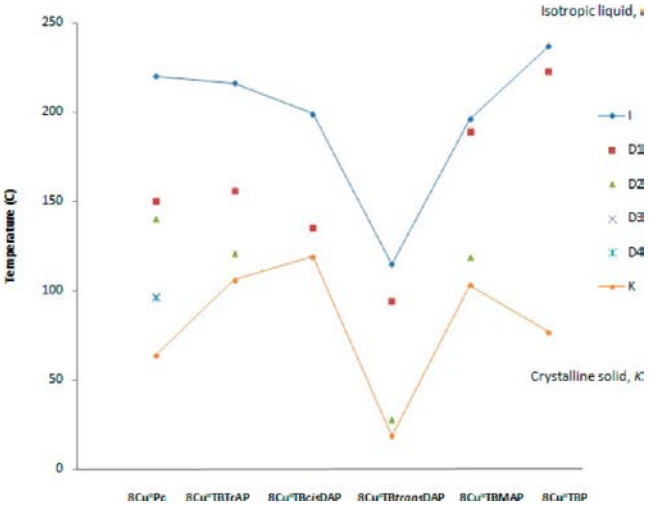

Figure 5. Transition temperatures for the series of octaoctyltetrabenzo(aza)porphyrin copper derivatives. Data for the Pc analogue is taken from ref 13.

$^1/_2$, as is the case with d^9 Cu^{II} complexes, this is not expected to be a factor with the partially aza-fused compounds because the D_{2h} and C_{2v} symmetries break the orbital degeneracy of the $\pi\pi^*$ excited states. Although application of TD-DFT to the three Faraday terms has recently been developed using the *Amsterdam Density Functional Suite*,[17] MCD spectra cannot currently be calculated using the commercially available form of the *Gaussian* software package. Older theoretical approaches for describing the electronic structures of porphyrinoids, such as Gouterman's four-orbital model[18] and Michl's perimeter model,[11] can be used to provide a conceptual framework for validating the results of theoretical calculations based on the relative energies of the frontier π molecular orbitals (MOs) in a manner that is readily accessible to the experimentalist in conceptual terms. Moffitt[19] and Michl[11] demonstrated that the relative intensities of the major electronic absorption bands of aromatic π systems can be successfully described in terms of perturbations to the structure of a high-symmetry parent hydrocarbon ($C_{16}H_{16}^{2-}$ in the case of metal tetrapyrrole porphyrinoid complexes or $C_{18}H_{18}$ for free-base compounds). The nodal patterns of the π-system MOs are retained even when the symmetry of the cyclic perimeter is modified. As a consequence of this, there is an M_L = 0, ±1, ±2, ±3, ±4, ±5, ±6, ±7, and 8 sequence in ascending energy terms in the π MOs of metal porphyrinoids (Figure 6), in a manner analogous

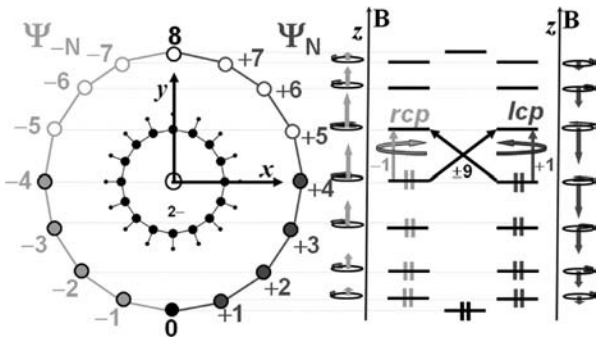

Figure 6. Michl's perimeter model[11] for $C_{16}H_{16}^{2-}$ (left). The circle represents a diagrammatic representation of the clockwise and counterclockwise motion of π-system electrons on the inner ligand perimeter generating the M_L value for each complex π MO. The alignment and magnitude of the magnetic moments induced by the electron motion within each π MO (center) can be predicted based on the right-hand rule and linear combination of atomic orbitals calculations. The moments aligned along the z axis with or against the applied field are shown diagrammatically.[11] Right and left handedness is defined within classical optics looking toward the light source of the circular dichroism spectrometer (lcp and rcp = left and right circularly polarized light).

to that of the M_L = 0, ±1, ±2, and 3 π-MO sequence, that forms the basis of the aromatic properties of benzene. Within the band nomenclature of Gouterman's four-orbital model,[18] there is an electronically allowed B transition and a forbidden Q transition linking the frontier M_L = ±4, ±5 π MOs based, respectively, on ΔM_L = ±1 and ±9 transitions. When a structural perturbation results in a marked lifting of the degeneracy of the MOs derived from the highest occupied molecular orbital (HOMO) and/or lowest unoccupied molecular orbital (LUMO) of the parent perimeter (referred

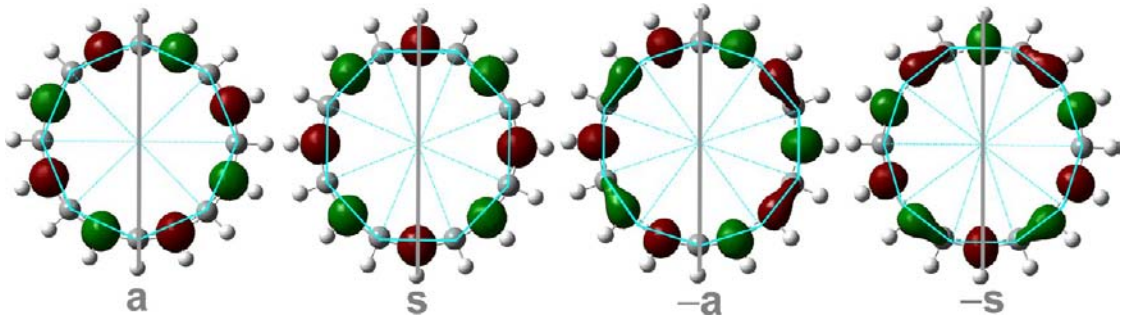

Figure 7. In Michl's perimeter model,[11] the nodal properties of the frontier π MOs on the inner perimeter of porphyrinoid ligands understood based on a $C_{16}H_{16}^{2-}$ parent hydrocarbon. Gray and black are used to denote the phase changes in the isosurfaces of the MO at 0.04 au. The 2*N* nodal planes of the MOs derived from the HOMO of a 4*N*+2 parent perimeter typically form octagons on the perimeter, with the planes running through alternating atoms, while the 2(*N* + 1) nodal planes of the LUMO-level MOs form a decagon in which, with the exception of those lying on either the *x* or *y* axis, the nodes and antinodes do not coincide with the atom positions. With a symmetry-lowering perturbation such as fused-ring expansion or core modification, the nodal patterns are determined by the alignment of the plane of symmetry in the *yz* plane. Michl introduced **a**, **s**, −**a**, and −**s** nomenclature to describe the four frontier π MOs in this context based on whether there is a nodal plane (**a** and −**a**) or an antinode (**s** and −**s**) on what corresponds to $M_L = 0$ in Figure 6. Similar nodal patterns can be observed for the four frontier π MOs of the copper(II) complexes of TBP, TBMAP, TB*trans*DAP, TB*cis*DAP, TBTrAP and Pc (Figure 9). Once the alignment of the nodal planes has been clearly defined, the effect of different structural perturbations can be readily conceptualized on a qualitative basis through consideration of the relative size of the MO coefficients on each atom on the perimeter.

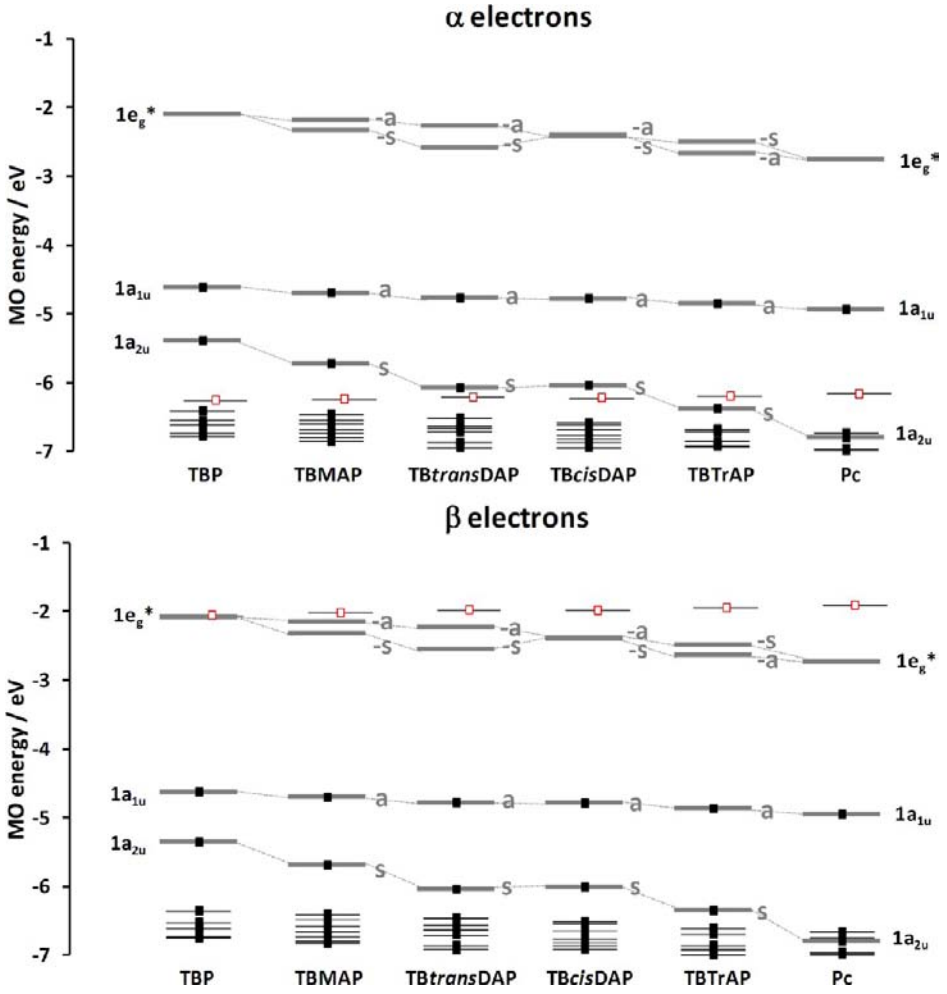

Figure 8. MO energies predicted for the copper(II) complexes of TBP, TBMAP, TB*trans*DAP, TB*cis*DAP, TBTrAP, and Pc in B3LYP geometry optimizations with 6-31G(d) basis sets. Occupied MOs are denoted with black squares, while the MO derived primarily from the partially occupied d_{z2} MO of the central metal is highlighted with an open red square and is offset to the right along with other MOs that are not associated with the ligand π system. The four frontier π MOs associated with Gouterman's four-orbital model[18] are highlighted with thicker and wider gray lines.

dx.doi.org/10.1021/ic301712h | *Inorg. Chem.* 2012, 51, 12820−12833

Table 3. Calculated Electronic Excitation Spectra of Cu^{II}Pc, Cu^{II}TBTrAP, Cu^{II}TB*cis*DAP, Cu^{II}TB*trans*DAP, Cu^{II}TBMAP, and Cu^{II}TBP Based on TD-DFT Calculations Using the B3LYP Functional and with 6-31G(d) Basis Sets

Cu^{II}Pc (D_{4h})								
band[a]	no.[b]	sym[c]	calcd[d]			exptl[e],[12]		wave function[f]
	1	$^1A_{1g}$						ground state
Q	**4** and **5**	^1E_u	16.9	592	(0.40)	14.2	706	38% **a** → $1e_g^{*A}$; 35% **a** → $1e_g^{*B}$; ...
B1	**48** and **49**	^1E_u	29.9	335	(0.25)	28.7	348	30% **a** → $1e_g^{*A}$; 30% **a** → $1e_g^{*B}$; 13% $2a_{2u}$ → $1e_g^{*B}$; 11% $2a_{2u}$ → $1e_g^{*A}$; ...
B2	**51** and **52**	^1E_u	30.4	329	(0.28)	28.7	348	43% $1b_{1u}$ → $1e_g^{*B}$; 36% $1b_{1u}$ → $1e_g^{*A}$; ...
Cu^{II}TBTrAP (C_{2v})								
band[a]	#[b]	sym[c]	calcd[d]			exptl[e]		wave function[f]
	1	$^1A_1$						ground state
Q	**4**	$^1A_1$	16.8	594	(0.39)	14.2	703	38% **a** → $-\mathbf{a}^B$; 35% a → $-\mathbf{a}^A$; 4% s → $-\mathbf{s}^A$; 5% s → $-\mathbf{s}^B$; ...
Q	**6**	$^1B_1$	17.5	572	(0.32)	14.8	676	39% **a** → $-\mathbf{s}^B$; 36% **a** → $-\mathbf{s}^A$; 7% **s** → $-\mathbf{a}^B$; 6% **s** → $-\mathbf{a}^A$; ...
B1	**23**	$^1B_1$	26.8	373	(0.08)	24.9	402	32% $2b_2(1e_g)$ → $-\mathbf{a}^A$; 15% $2a_2(1e_g)$ → $-\mathbf{s}^{*A}$; 14% **a** → $-\mathbf{a}^B$; 14% **s** → $-\mathbf{a}^A$; 13% $2b_2(1e_g)$ → $-\mathbf{a}^{*A}$; ...
	31	$^1B_1$	28.0	357	(0.24)			14% **a** → $2b_2^{*A}$; 13% **s** → $-\mathbf{a}^A$; 12% **s** → $2b_2^{*B}$; 12% $2b_2(1e_g)$ → $-\mathbf{a}^{*A}$; 10% **s** → $-\mathbf{s}^B$; ...
	43	$^1B_1$	29.4	341	(0.25)			19% **a** → $2b_2^{*B}(1b_{1u}^*)$; 17% **a** → $2b_2^{*A}(1b_{1u}^*)$; ...
B1	**44**	$^1A_1$	29.4	340	(0.20)	26.1	383	24% **s** → $-\mathbf{s}^B$; 20% **s** → $-\mathbf{s}^A$; 11% $2b_2(1e_g)$ → $-\mathbf{s}^{*A}$; ...
	46	$^1A_1$	29.8	336	(0.21)			22% $2b_2(1e_g)$ → $-\mathbf{s}^{*A}$; 20% $2b_2(1e_g)$ → $-\mathbf{s}^{*B}$; ...
Cu^{II}TB*cis*DAP (C_{2v})								
band[a]	#[b]	sym[c]	calcd[d]			exptl[e]		wave function[f]
	1	$^1A_1$						ground state
Q	**5**	$^1A_1$	17.4	573	(0.31)	14.9	673	39% **a** → $-\mathbf{a}^B$; 36% **a** → $-\mathbf{a}^A$; 8% s → $-\mathbf{s}^B$; 7% **s** → $-\mathbf{s}^A$; ...
Q	**6**	$^1B_1$	17.5	572	(0.30)	15.2	658	39% **a** → $-\mathbf{s}^B$; 35% **a** → $-\mathbf{s}^A$; 9% **s** → $-\mathbf{a}^B$; 7% **s** → $-\mathbf{a}^A$; ...
B	**25**	$^1B_1$	27.3	366	(0.44)	24.8	403	30% **s** → $-\mathbf{a}^A$; 24% **s** → $-\mathbf{a}^B$; ...
B	**28**	$^1A_1$	27.9	358	(0.54)	26.1	383	30% **s** → $-\mathbf{s}^A$; 27% **s** → $-\mathbf{s}^B$;
Cu^{II}TB*trans*DAP (D_{2h})								
band[a]	#[b]	sym[c]	calcd[d]			exptl[e]		wave function[f]
	1	^1A_g						ground state
Q	**5**	$^1B_{3u}$	16.8	597	(0.38)	14.3	698	38% **a** → $-\mathbf{s}^B$; 35% **a** → $-\mathbf{s}^A$; 6% **s** → $-\mathbf{a}^A$; 6% **s** → $-\mathbf{a}^B$; ...
Q	**6**	$^1B_{2u}$	17.9	557	(0.21)	15.3	655	39% **a** → $-\mathbf{a}^B$; 35% **a** → $-\mathbf{a}^A$; 13% **s** → $-\mathbf{s}^B$; 10% **s** → $-\mathbf{s}^A$; ...
B	**25**	$^1B_{2u}$	27.3	366	(1.00)	23.8	420	31% **s** → $-\mathbf{s}^A$; 30% **s** → $-\mathbf{s}^B$; ...
B	**39**	$^1B_{3u}$	29.4	340	(0.52)	26.7	374	34% **s** → $-\mathbf{a}^A$; 32% **s** → $-\mathbf{a}^B$; ...
Cu^{II}TBMAP (C_{2v})								
band[a]	#[b]	sym[c]	calcd[d]			exptl[e]		wave function[f]
	1	$^1A_1$						ground state
Q	**5**	$^1B_1$	17.4	576	(0.29)	14.2	703	38% **a** → $-\mathbf{s}^B$; 35% **a** → $-\mathbf{s}^A$; 10% **s** → $-\mathbf{a}^A$; 8% **s** → $-\mathbf{a}^B$; ...
Q	**6**	$^1A_1$	17.9	559	(0.20)	14.8	676	37% **a** → $-\mathbf{a}^B$; 35% **a** → $-\mathbf{a}^A$; 17% **s** → $-\mathbf{s}^B$; 7% **s** → $-\mathbf{s}^A$; ...
B	**23**	$^1A_1$	26.9	372	(0.95)	24.9	402	30% **s** → $-\mathbf{s}^B$; 30% **s** → $-\mathbf{s}^A$; ...
B	**25**	$^1B_1$	27.4	365	(0.65)	26.1	383	30% **s** → $-\mathbf{a}^B$; 30% **s** → $-\mathbf{a}^A$; ...
Cu^{II}TBP (D_{4h})								
band[a]	#[b]	sym[c]	calcd[d]			exptl[e],[20]		wave function[f]
	1	$^1A_{1g}$						ground state
Q	**9** and **10**	^1E_u	17.8	563	(0.12)	15.2	660	52% **s** → $1e_g^{*A}$; 17% **a** → $1e_g^{*A}$; 32% **a** → $1e_g^{*B}$; ...
B	**22** and **23**	^1E_u	26.4	379	(0.95)	23.3	429	29% **s** → $1e_g^{*A}$; 28% **s** → $1e_g^{*B}$; ...

[a]Band assignment described in the text. [b]The number of the state assigned in terms of ascending energy within the TD-DFT calculation. [c]The state symmetry. [d]Calculated band energies (10^3 cm^{-1}), wavelengths (nm), and oscillator strengths in parentheses (*f*). [e]Observed energies (10^3 cm^{-1}) and wavelengths (nm). [f]The wave functions based on the eigenvectors predicted by TD-DFT. One-electron transitions associated with the four frontier π MOs of Gouterman's four-orbital model[18] are highlighted in bold.

to as the ΔHOMO and ΔLUMO values within Michl's terminology[11]), there is a mixing of the allowed and forbidden properties of the Q and B bands and a marked intensification of the Q band, which as a consequence can become the dominant spectral feature for some porphyrinoids such as the Pc's.[20,21] When ΔHOMO ≈ ΔLUMO, the Q bands remain relatively weak because the orbital angular momentum properties of the parent hydrocarbon perimeter are retained and the absorption intensity in the Q band region is based primarily on vibrational borrowing from the allowed B(0,0) bands.[22]

Michl[11] introduced the **a**, **s**, −**a**, and −**s** terminology for the four MOs derived from the HOMO and LUMO of the parent perimeter so that π systems of porphyrinoids with differing molecular symmetry and relative orderings of the four frontier π MOs in energy terms can be readily compared. One MO derived from the HOMO of the parent perimeter and another derived from the LUMO have nodal planes that coincide with

dx.doi.org/10.1021/ic301712h | *Inorg. Chem.* 2012, 51, 12820−12833

the *yz* plane and are referred to respectively as the **a** and −**a** MOs, while the corresponding MOs with antinodes on the *yz* plane are referred to as the **s** and −**s** MOs. The HOMO level of $4N + 2$ π-electron systems have $2N$ nodal planes, while the LUMO levels have $2(N + 1)$, effectively forming an octagon or a decagon on the 16-atom inner perimeter (Figure 7). The D_{4h} symmetry of the porphyrin dianion dictates that the −**a** and −**s** MOs are degenerate because the $M_L = \pm 5$ nodal patterns differ along the *x* and *y* axes only by being rotated by 90° with respect to each other. In the context of Gouterman's four-orbital model, the symmetry-split **a** and **s** MOs of D_{4h} symmetry MPc complexes transform as a_{1u} and a_{2u}, respectively, while the −**a** and −**s** MOs form the doubly degenerate e_g* LUMO.[18] The MCD spectrum is, therefore, usually dominated by Faraday $\mathcal{A}_1$ terms because the ground state is orbitally nondegenerate and the Q and B excited states are orbitally degenerate.

B3LYP-optimized geometries calculated with 6-31G(d) basis sets for the copper(II) complexes of TBP, TBMAP, TB*cis*DAP, TB*trans*DAP, TBTrAP, and Pc can be used to analyze trends in the energies of the frontier π MOs (Figure 8). Earlier ZINDO calculations for the dianion species of TBMAP, TB*cis*DAP, TB*trans*DAP, and TBTrAP[16] revealed that partial aza substitution causes a comparatively minor perturbation to the electronic structure of TBP, based primarily on the electronegativity difference between *meso*-carbon and aza-nitrogen atoms. Trends in the energies and intensities of the Q and B bands (Figure 14 and Table 3) can be readily rationalized using Michl's perimeter model.[11] The isosurfaces of the **a**, **s**, −**a**, and −**s** MOs demonstrate that there is relatively little mixing with the d MOs of the central Cu^{II} ion in the DFT calculations (Figure 9). The Q band shifts ca. 40 nm to the red upon moving from Cu^{II}TBP to Cu^{II}Pc, which points to a significant narrowing of the HOMO−LUMO band gap. The narrowing of the HOMO−LUMO band gap is primarily associated with the 0.65 eV stabilization of the LUMO (the −**s** MO) upon moving from Cu^{II}TBP to Cu^{II}Pc due to the large MO coefficients at the meso positions (Figures 8 and 9). This leads to a narrowing of the HOMO−LUMO band gap and hence to a slight red shift of the Q band because the energy of the HOMO, which is the **a** MO, is only stabilized by 0.32 eV (Figure 9).

The **s** MO is steadily stabilized with the addition of each successive aza-nitrogen atom because there are large MO coefficients at the meso positions (Figures 8 and 9) and moves from being HOMO−1 in the context of Cu^{II}TBP to HOMO−5 in the context of the α electrons of Cu^{II}Pc. The ΔHOMO values become progressively larger, with the addition of each aza-nitrogen atom ranging between 0.78 eV for Cu^{II}TBP and 1.87 eV for Cu^{II}Pc (Figure 9), because the meso positions lie on nodal planes in the context of the **a** MO and hence are not affected as significantly by this structural modification. The UV/vis absorption and MCD spectra of TBTrAP compounds[16] are, therefore, similar to those of M^{II}Pcs (Figures 3 and 10),[20] while the spectra of TBMAP are similar to those of TBP (Figures 3 and 13). The most important feature to note in this regard is that there is a significant red shift and relative intensification of the B band as the ΔHOMO value increases over the series of compounds from Cu^{II}Pc to Cu^{II}TBP (Figure 14), while in the Q band region, there is a blue shift and relative decrease in the band intensity. The blue shift of the B band can be readily explained using Michl's perimeter model,[11] based on stabilization of the **s** MO relative to the −**a** and −**s** MOs (Figure 8) as aza-nitrogen atoms are added to the structure, because the **s** → −**a** and **s** → −**s** one-electron transitions

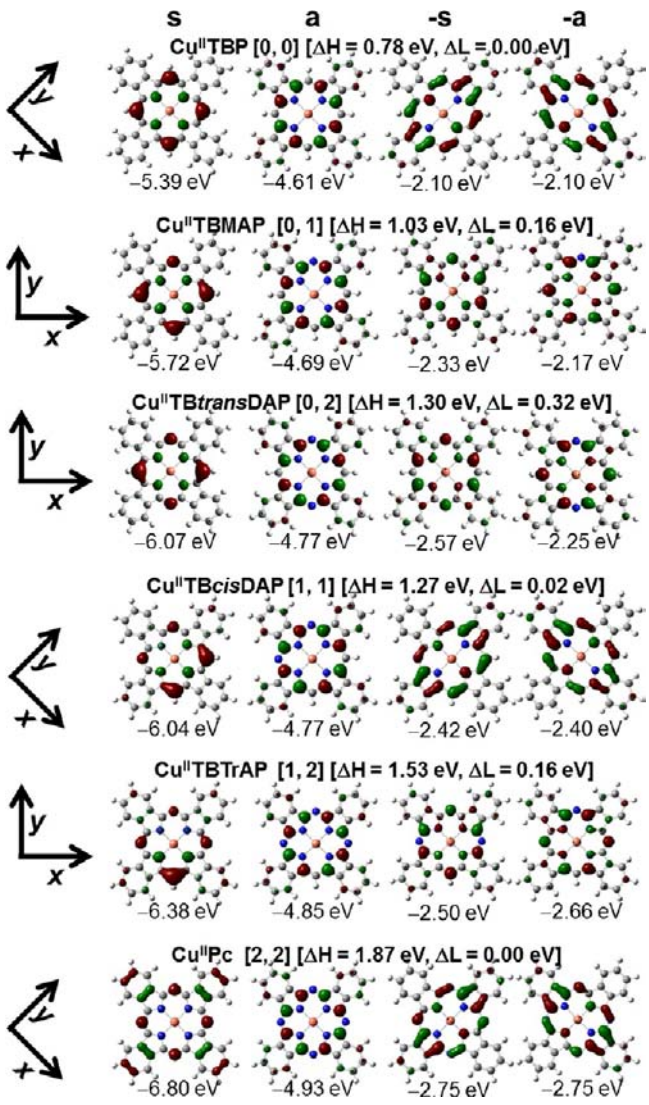

Figure 9. Nodal patterns of the **a**, **s**, −**a**, and −**s** MOs of copper(II) complexes of TBP, TBMAP, TB*trans*DAP, TB*cis*DAP, TBTrAP, and Pc in B3LYP geometry optimizations with 6-31G(d) basis sets at an isosurface value of 0.04 au. The *x* and *y* axes of TBP, TB*cis*DAP, and Pc are rotated by 45° relative to those of TBMAP, TB*trans*DAP, and TBTrAP, so the nodal patterns of the −**a** and −**s** MOs differ markedly. The **a**, **s**, −**a**, and −**s** MOs are defined based on the presence and absence of nodal planes on the meso atoms along the *y*-axis alignment of TBMAP, TB*trans*DAP, and TBTrAP. The number of aza nitrogen atoms that lie along the *x* and *y* axes, respectively, within this axis alignment are provided in parentheses for each compound. The stabilizing effect on the −**a** and/or −**s** MOs when there are large MO coefficients on aza-nitrogen atoms is reflected in the relative energies predicted for these MOs for the TBMAP, TB*trans*DAP, and TBTrAP complexes in Figure 8 and in the markedly different ΔLUMO values predicted for the TB*trans*DAP and TB*cis*DAP complexes. The ΔHOMO (ΔH) and ΔLUMO (ΔL) values are provided for each compound in a second set of parentheses.

provide the dominant contributions to the B excited states (Table 3). It has also previously been demonstrated in the context of a series of radially symmetric fused-ring-expanded zinc(II) porphyrinoids[25] that when the ΔHOMO value of fused-ring-expanded porphyrinoids increases, there is a mixing of the allowed and forbidden properties of the Q and B bands and a greater level of configuration interaction between the B

dx.doi.org/10.1021/ic301712h | *Inorg. Chem.* 2012, 51, 12820−12833

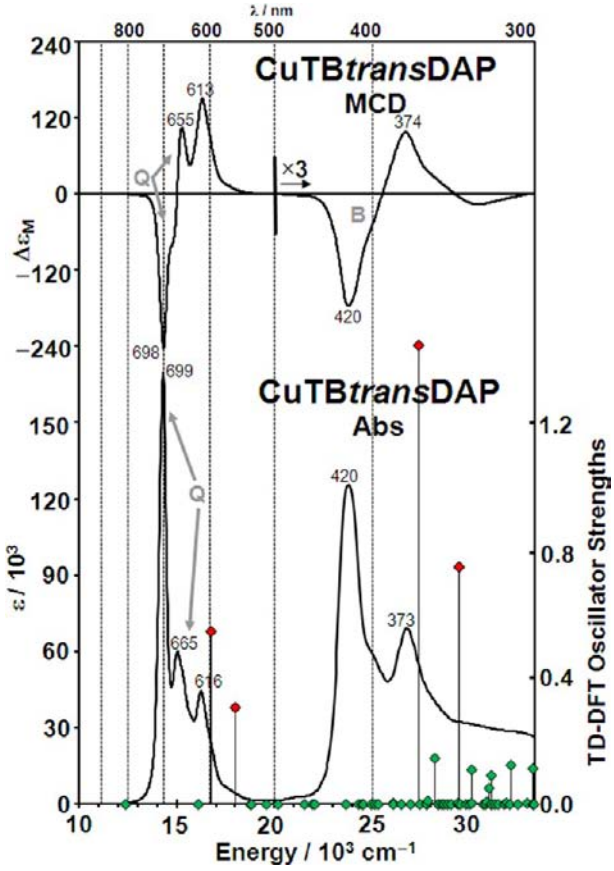

Figure 10. Absorption and MCD spectra of 8Cu^{II}TBTrAP in $CHCl_3$ with the calculated TD-DFT spectrum plotted against a secondary axis using diamonds to denote the oscillator strength of each band. Red diamonds are used to highlight the Q(0,0) and B(0,0) bands, which have the largest contributions from the four spin-allowed one-electron transitions in Gouterman's four-orbital model.[18].

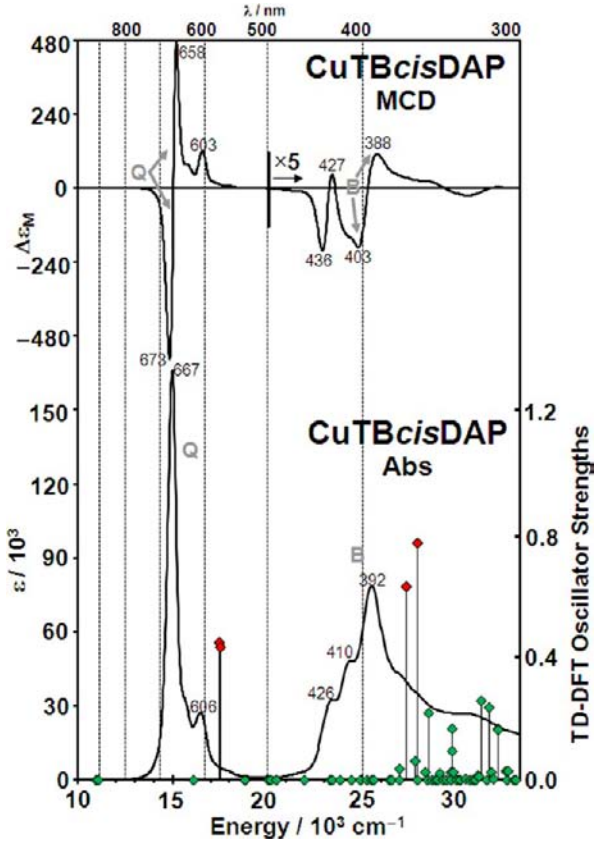

Figure 11. Absorption and MCD spectra of 8CuTB*cis*DAP in $CHCl_3$ with the calculated TD-DFT spectrum plotted against a secondary axis using diamonds to denote the oscillator strength of each band. Red diamonds are used to highlight the Q(0,0) and B(0,0) bands, which have the largest contributions from the four spin-allowed one-electron transitions in Gouterman's four-orbital model.[18]

and higher-energy $\pi\pi^*$ states (Table 3). In the context of Pc's, MCD studies have demonstrated that there are two intense overlapping derivative-shaped Faraday $\mathcal{A}_1$ terms in the B-band region.[20,26] Gouterman's Q and B band nomenclature was, therefore, modified to include B1 and B2 bands.[18] The B1 and B2 band terminology is used in assigning the spectra of Cu^{II}TBTrAP based on the presence of two coupled pairs of oppositely signed $\mathcal{B}_0$ terms, which replace the $\mathcal{A}_1$ terms due to C_{2v} symmetry.[15] As has been observed previously,[24] the B bands of the TBMAP compound are sharper and more intense than those in the spectra of TBTrAP and Pc compounds and shift to longer wavelength at ca. 400 nm. There is a lower degree of mixing of the allowed and forbidden properties of the Q and B band transitions and hence weaker absorbance in the Q band region relative to the B band (Figures 3 and 13) because of the significantly lower ΔHOMO value (Figure 9).

Luk'yanets and co-workers[8] reported earlier the marked differences in the spectra of TB*cis*DAP and TB*trans*DAP compounds, and these differences are also evident in the spectra of the present derivatives shown in Figures 3, 11, and 12. A comparison between the coupled pair of oppositely signed Faraday $\mathcal{B}_0$ terms in the MCD spectrum and the corresponding bands in the UV/vis absorption spectrum makes it clear that there is a marked zero-field splitting of the Q(0,0) bands of Cu^{II}TB*trans*DAP. The negative $\mathcal{B}_0$ term at 699 nm is closely aligned with the intense absorption band at 698 nm, and the corresponding positive $\mathcal{B}_0$ term lies at 655 nm. The perturbation to the structure varies along the *x* and *y* axes in a manner that corresponds with the differing alignments of the nodal planes of the **−a** and **−s** MOs (Figure 7). A significant ΔLUMO value is, therefore, anticipated because the two aza-nitrogen atoms lie on a nodal plane in the **−a** MO but have significant MO coefficients in the **−s** MO (Figures 9 and 10). In contrast, despite the lack of a 3-fold or higher axis of symmetry, the Q band region of the MCD spectrum of Cu^{II}TB*cis*DAP can be viewed as being dominated by a pseudo-$\mathcal{A}_1$ term because the main absorption band at 667 nm lies close to the zero-intensity point of the derivative-shaped signal in the MCD spectrum, which is the pattern that would normally be anticipated for an $\mathcal{A}_1$ term. No splitting is observed for the Q(0,0) bands of the Cu^{II}TB*cis*DAP complex (Figure 11) because, as has previously been predicted on the basis of the symmetry-adapted perturbation method,[23] the perturbations to the structure are identical along the *x* and *y* axes. There is one aza-nitrogen atom and one *meso*-carbon atom along each axis (Figure 10), so incorporating the aza-nitrogen atoms would have an identical effect on the energies of the **−a** and **−s** MOs. The predicted ΔLUMO value is only 0.02 eV (Figure 9), so only a minor splitting of the Q and B bands into *x*- and *y*-polarized components is anticipated based on the DFT calculations. There are also marked differences between the spectra of Cu^{II}TB*cis*DAP and Cu^{II}TB*trans*DAP in the B band region. The MCD spectrum of Cu^{II}TB*cis*DAP contains two

dx.doi.org/10.1021/ic301712h | *Inorg. Chem.* 2012, 51, 12820−12833

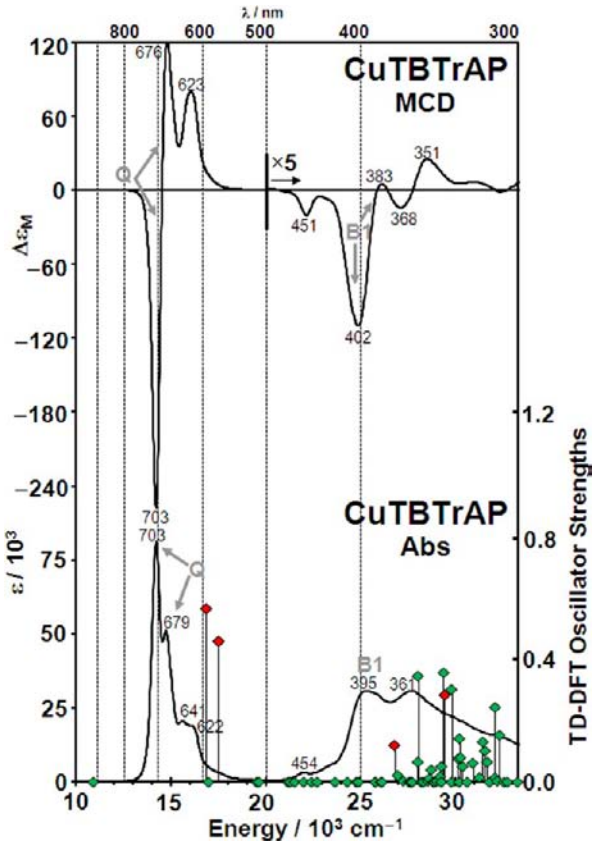

Figure 12. Absorption and MCD spectra of 8Cu^{II}TB*trans*DAP in $CHCl_3$ with the calculated TD-DFT spectrum plotted against a secondary axis using diamonds to denote the oscillator strength of each band. Red diamonds are used to highlight the Q(0,0) and B(0,0) bands, which have the largest contributions from the four spin-allowed one-electron transitions in Gouterman's four-orbital model.[18]

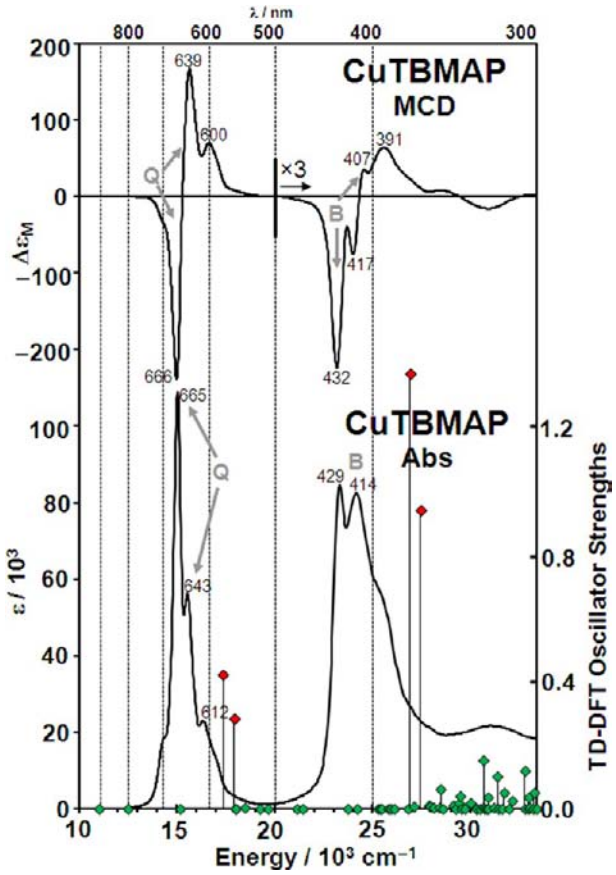

Figure 13. Absorption and MCD spectra of 8Cu^{II}TBMAP in $CHCl_3$ with the calculated TD-DFT spectrum plotted against a secondary axis using diamonds to denote the oscillator strength of each band. Red diamonds are used to highlight the Q(0,0) and B(0,0) bands, which have the largest contributions from the four spin-allowed one-electron transitions in Gouterman's four-orbital model.[18].

pairs of relatively well-resolved oppositely signed Faraday $\mathcal{B}_0$ terms, which could be viewed as pseudo-$\mathcal{A}_1$ terms, while that of Cu^{II}TB*trans*DAP is dominated by a pair of broader $\mathcal{B}_0$ terms, with a significantly larger energy separation between the minima and maxima of the negatively and positively signed bands. The difference between the spectra is related to the differing ΔLUMO values because this affects the configuration interaction between the higher-energy $\pi\pi^*$ states. We tentatively assign the 420 and 373 nm bands in the Cu^{II}TB*trans*DAP spectrum to the B transition because the TD-DFT calculation predicts a single set of intense bands in this region of the spectrum (Figure 12).

In the MCD spectra, the sign sequence with ascending energy observed in the Faraday $\mathcal{B}_0$ terms associated with the Q and B band transitions is consistently −/+/−/+ for the complete series of partially aza-substituted compounds (Figures 10−13). Because no significant mixing is predicted between the Q and B band transitions and ligand-to-metal or metal-to-ligand charge-transfer transitions associated with the d^9 configuration of the Cu^{II} central metal ion (Table 3), the −/+ sign sequence with ascending energy that would normally be anticipated for the Q and B bands of porphyrinoids with ΔHOMO ≫ ΔLUMO is retained. The ΔHOMO and ΔLUMO values can be regarded as measures of the extents to which circulation on the perimeter of the positively charged hole left in the HOMO and the negatively charged electron in the LUMO upon electronic excitation is hindered because of the lower symmetry relative to the parent hydrocarbon perimeter.[11,15] This determines the alignment of the induced magnetic dipole moments of the Q and B band excited states relative to the applied magnetic field and hence whether there is net absorption of left or right circularly polarized light associated with each band. Even in the context of Cu^{II}TB*trans*DAP, which has the largest structural perturbation along the *x* and *y* axes, the predicted ΔLUMO value of 0.32 eV remains considerably lower than the corresponding ΔHOMO value of 1.30 eV (Figures 8 and 9).

EXPERIMENTAL SECTION

Equipment. ^{1}H NMR spectra at 300 and 400 MHz were recorded on a Varian Gemini 300 spectrometer and a Varian 400 Lambda spectrometer, respectively. Signals are quoted in ppm as δ downfield from tetramethylsilane (δ = 0.00). At University of East Anglia, ultraviolet spectra were recorded using a Hitachi U-3000 spectrophotometer. Mass analysis was undertaken using a Shimadzu MALDI-TOF-MS spectrometer with a TA1586Ade plate and DCTB as the matrix and calibrated against 1,4,8,11,15,18,22,25-octaoctylphthalocyanine.

At Tohoku University, electronic absorption spectra were measured with a Jasco V-570 spectrophotometer. MCD spectra were recorded using a Jasco J-725 spectrodichrometer and a Jasco electromagnet that produces a magnetic field of up to 1.09 T. The sign conventions of Piepho and Schatz are adopted when describing the three Faraday terms.[27]

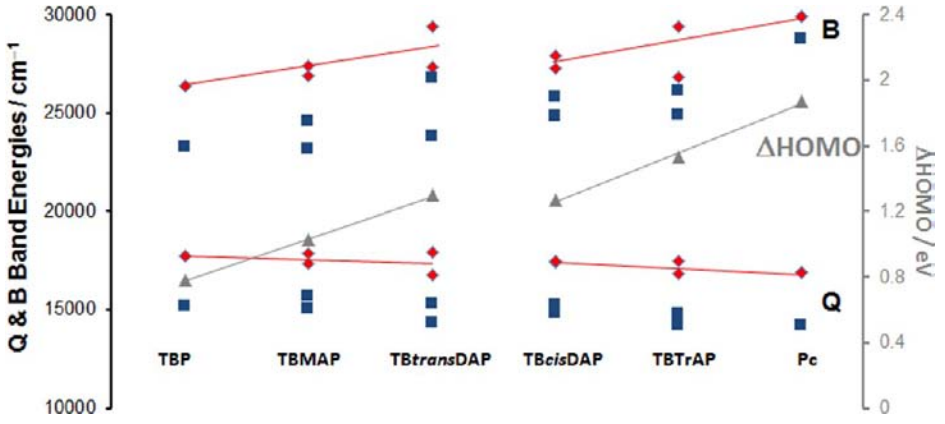

Figure 14. Trends in the calculated (red diamonds) and observed (blue squares) energies of the Q and B bands for the copper(II) complexes of TBP, TBMAP, TB*trans*DAP, TB*cis*DAP, TBTrAP, and Pc. The calculated ΔHOMO values are plotted against a secondary axis (gray triangles).

Phase and mesophase transition temperatures were observed through an Olympus BH2 polarizing optical microscope fitted with a Linkham THM60 hotstage operating at a heating and cooling rate of 5 °C·min^{-1}. Temperatures were confirmed by differential scanning calorimetry using a Q20 TA DSC instrument with heating and cooling rates of 2 °C·min^{-1}.

Elemental analyses were undertaken by London Metropolitan University. Thin-layer chromatography analysis was carried out on Merck aluminum-backed silica gel 60 F254 coated plates and visualized under normal light. Column chromatography was performed at ambient temperature using Davisil chromatographic silica media LC60 Å 40−63 μm, with solvent systems given as volume ratios.

X-ray diffraction was performed by the UK National Crystallography Service at 119 Beamline, Diamond Light Source, according to a previously published procedure.[28] Cell determination, data collection, and treatment were undertaken using *CrystalClear-SM Expert* 2.0 r7 (Rigaku, 2011). Structure solution was achieved using *SUPERFLIP* and refined using *SHELXL97*.

Materials. Methylmagnesium bromide (MeMgBr) as 3.0 M solutions in THF was supplied by Aldrich. The preparation of 3,6-dioctylphthalonitrile has been described elsewhere.[12]

Compound Synthesis. *General Procedure for the Synthesis of 1,4,8,11,15,18,22,25-Octaoctyltetrabenzo[b,g,l,q](aza)-porphinatomagnesium Derivatives.* 3,6-Dioctylphthalonitrile (200.0 mg, 0.567 mmol) was dissolved in dry THF (3.0 mL) under an argon atmosphere. The solution was stirred at room temperature, and *n* mL (*n* varies according to the number of equivalents used) of a 3.0 M solution of MeMgBr was added dropwise via a syringe. The reaction mixture was immersed in an oil bath and heated under reflux for 30 min. During this time, the mixture changes from a colorless solution to dark blue/purple or mauve depending on the number of equivalents of Grignard reagent used. The vessel was removed from heating and left to cool to room temperature, while the remaining solvent was evaporated by a stream of argon. Distilled/degassed quinoline (3.0 mL) was added to the vessel via a syringe, and the reaction mixture was heated to reflux (≈200 °C) for 3 h under argon. After cooling, the majority of quinoline was removed under reduced pressure, methanol (MeOH) added, and the crude product mixture dispersed using an ultrasonic bath. The resulting suspension was passed through a silica plug and flushed with MeOH to remove the remaining quinoline and other polar impurities. Once the filtrate appeared colorless, THF was added to flush out a dark-green fraction. In one set of experiments, the mixture was separated by atmospheric-pressure column chromatography over silica gel [dichloromethane (DCM) eluent] to give the various magnesium-metalated derivatives as amorphous viscous gums. In addition, a sample of the dark-green fraction was analyzed by ^{1}H NMR spectroscopy to establish the composition of the mixture of macrocyclic products (see the text).

1,4,8,11,15,18,22,25-Octaoctyltetrabenzo[b,g,l,q][5,10,15]-triazaporphinatomagnesium (8MgTBTrAP). Using the general procedure above (2 equiv of MeMgBr), the *title compound* was separated as the first fraction as a dark-green semisolid (0.061g, 30%). MALDI-MS: isotopic cluster at *m*/*z* 1433.05 [100%, M$^+$]. ^{1}H NMR (400 MHz, toluene-d^8): δ 11.23 (s, 1H), 7.98 (s, 4H), 7.93 (bd, 2H), 7.87 (bd, 2H), 5.10−4.92 (m, 12H), 4.33 (bt, 4H), 2.62−2.34 (m, 16H), 1.96−1.74 (m, 16H), 1.40−0.91 (m, 64H), 1.03−0.74 (m, 24H). UV/vis (in THF): λ = 694 nm.

1,4,8,11,15,18,22,25-Octaoctyltetrabenzo[b,g,l,q][5,10] and -[5,15]diazaporphinatomagnesium (8MgTBcisDAP and 8MgTBtransDAP). Two additional fractions were recovered as dark-green viscous gums from the separation above and identified as the cis and trans isomers. However, larger amounts of the two isomers were obtained using 3 equiv of MeMgBr. Cis isomer (from 3.0 equiv to 0.011 g, 5% yield). MALDI-MS: isotopic cluster at *m*/*z* 1432.41 [100%, M$^+$]. ^{1}H NMR (400 MHz, toluene-d^8): δ 11.32 (s, 2H), 8.03 (s, 2H), 7.99 (bd, 2H), 7.95 (bd, 2H), 7.83 (s, 2H), 5.22−5.01 (m, 8H), 4.42 (bt, 8H), 2.64−2.39 (m, 16H), 2.02−1.72 (m, 16H), 1.48−1.32 (m, 80H), 1.07−0.76 (m, 24H). UV/vis (in THF): λ = 633 nm. Trans isomer (from 3.0 equiv to 0.012 g, 6% yield). ^{1}H NMR (400 MHz, toluene-d^8): δ 11.39 (s, 2H), 8.02 (d, *J* = 7.3 Hz, 4H), 7.95 (d, *J* = 7.3 Hz, 4H), 5.16 (bt, 8H), 4.47 (bt, 8H), 2.68−2.44 (m, 16H), 1.98−1.74 (m, 16H), 1.48−1.30 (m, 80H), 0.98−0.77 (m, 24H). UV/vis (in THF): λ = 691 nm.

1,4,8,11,15,18,22,25-Octaoctyltetrabenzo[b,g,l,q][5]-monoazaporphinatomagnesium (8MgTBMAP). After elution of the first two bands, the TBDAP derivatives, the *title compound* was eluted as the main fraction to give a bright-green viscous solid (from 3.0 equiv to 0.036 g, 18%). MALDI-MS: isotopic cluster at *m*/*z* 1431.46 [100%, M$^+$]. ^{1}H NMR (400 MHz, toluene-d^8): δ 11.60 (s, 1H), 11.46 (s, 2H), 8.09−7.96 (m, 4H), 7.92 (s, 4H), 5.37−5.15 (m, 8H), 4.56−4.15 (m, 8H), 2.60−2.46 (m, 16H), 1.97−1.73 (m, 16H), 1.47−1.29 (m, 64H), 1.01−0.78 (m, 24H). UV/vis (in THF): λ = 659 nm.

1,4,8,11,15,18,22,25-Octaoctyltetrabenzo[b,g,l,q]-porphinatomagnesium (8MgTBP). The TBP derivative was obtained by using both 3.0 and 4.0 equiv of MeMgBr using the general procedure. Using 4.0 equiv yielded the porphyrin as the major product, but the overall yield of the reaction was lower. In both cases, the product was obtained as the final band to be eluted from the silica gel column after changing the eluent (DCM/THF 50:1). The *title compound* was obtained after removal of the solvent as a black viscous gum (0.021 g, 10% from the experiment using 4 equiv of MeMgBr). MALDI-MS: isotopic cluster at *m*/*z* 1429.90 [100%, M$^+$]. ^{1}H NMR (400 MHz, toluene-d^8): δ 11.81 (s, 4H), 8.03 (s, 8H), 4.70 (t, *J* = 7.3 Hz, 16H), 2.81−2.51 (m, 16H), 2.02−1.30 (m, 80H), 0.89 (t, *J* = 7.3 Hz, 24H). UV/vis (in THF): λ = 641 nm.

General Procedure for Demetalation of 1,4,8,11,15,18,22,25-Octaoctyltetrabenzo[*b*,*g*,*l*,*q*](aza)-porphinatomagnesium Derivatives. In a typical procedure, the magnesium-metalated macrocycle was dissolved in glacial acetic acid and heated at reflux for 30 min. After cooling, the mixture was poured onto distilled water and the product extracted with hexanes. The

dx.doi.org/10.1021/ic301712h | *Inorg. Chem.* 2012, 51, 12820−12833

organic fraction was washed repeatedly with distilled water to remove traces of acid and finally with brine. The fraction was then dried with Na_2SO_4 and filtered and the solvent removed to give a residue that was purified by column chromatography over silica gel (DCM). Recrystallization of the fraction from DCM/MeOH gave the metal-free macrocycle.

1,4,8,11,15,18,22,25-Octaoctyltetrabenzo[b,g,l,q][5,10,15]-triazaporphyrin (8H$_2$TBTrAP). 1,4,8,11,15,18,22,25-Octaoctyltetrabenzo[*b*,*g*,*l*,*q*][5,10,15]triazaporphinatomagnesium (40.0 mg, 0.028 mmol) was demetalated in glacial acetic acid (20.0 mL) using the general procedure to afford the *title compound* as thin, threadlike crystals (14.6 mg, 37%). IR (cm^{-1}): ν 3299 (w, NH). MALDI-MS: isotopic cluster at *m*/*z* 1410.24 [100%, M$^+$]. ^{1}H NMR (400 MHz, toluene-*d*^{8}, 80 °C): δ 10.83 (s, 1H), 7.89 (s, 4H), 7.87−7.76 (m, 4H), 4.80 (t, *J* = 7.3 Hz, 4H), 4.74 (t, *J* = 7.1 Hz, 12H), 2.43−2.20 (m, 16H), 1.84−1.68 (m, 16H), 1.53−1.41 (m, 16H), 1.34−1.26 (m, 32H), 1.25−1.17 (m, 16H), 0.90−0.77 (m, 24H), 0.14 (s, 2H). UV/vis (in toluene): λ = 717 nm (log ε = 5.20). Thermotropic mesophase transitions (Cr, crystal phase; Col$_h$, hexagonal liquid crystal phase; I, isotropic liquid; data for the second heating and first cooling cycles): Cr 63 Col$_h$ 160 I 155 Col$_h$ 52 Cr (°C).

1,4,8,11,15,18,22,25-Octaoctyltetrabenzo[b,g,l,q][5,10]-diazaporphyrin (8H$_2$TBcisDAP). 1,4,8,11,15,18,22,25-Octaoctyltetrabenzo[*b*,*g*,*l*,*q*][5,10]diazaporphinatomagnesium (20.0 mg, 0.014 mmol) in glacial acetic acid (10.0 mL) afforded the *title compound* as small fine needlelike crystals (6.5 mg, 33%). IR (cm^{-1}): ν 3304 (w, NH). MALDI-MS: isotopic cluster at *m*/*z* 1409.28 [100%, M$^+$]. ^{1}H NMR (400 MHz, toluene-*d*^{8}, 80 °C): δ 11.02 (s, 2H), 7.90 (s, 2H), 7.86−7.80 (m, 4H), 4.88−4.73 (m, 8H), 4.28−4.15 (m, 8H), 2.47−2.33 (m, 8H), 2.32−2.22 (m, 8H), 1.83−1.70 (m, 16H), 1.52−1.37(m, 64H), 0.92−0.75 (m, 24H). UV/vis (in toluene): λ = 691 nm (log ε = 4.86). Thermotropic mesophase transitions (data for the second heating and first cooling cycles): Cr 67 Col$_h$ 166 I 163 Col$_h$ 59 Cr (°C).

1,4,8,11,15,18,22,25-Octaoctyltetrabenzo[b,g,l,q][5,15]-diazaporphyrin (8H$_2$TBtransDAP). 1,4,8,11,15,18,22,25-Octaoctyltetrabenzo[*b*,*g*,*l*,*q*][5,15]diazaporphinatomagnesium (20.0 mg, 0.014 mmol) in glacial acetic acid (10.0 mL) afforded the *title compound* as small fine needlelike crystals (6.9 mg, 35%). IR (cm^{-1}): ν 3295 (w, NH). MALDI-MS: isotopic cluster at *m*/*z* 1409.47 [100%, M$^+$]. ^{1}H NMR (400 MHz, toluene-*d*^{8}, 80 °C): δ 11.14 (s, 2H), 7.94 (d, *J* = 7.6 Hz, 4H), 7.88 (d, *J* = 7.6 Hz, 4H), 4.93 (t, *J* = 7.4 Hz, 8H), 4.28 (t, *J* = 7.2 Hz, 8H), 2.46−2.31 (m, 8H), 1.86−1.72 (m, 8H), 1.53−1.40 (m, 16H), 1.38−1.34 (m, 32H), 1.32−1.24 (m, 16H), 1.23−1.16 (m, 16H), 0.89−0.75 (m, 24H), −0.95 (s, 2H). UV/vis (in toluene): λ = 712 nm (log ε = 5.29). Thermotropic mesophase transitions (data for the second heating and first cooling cycles): Cr 85 Col$_h$ 165 I 161 Col$_h$ 74 Cr (°C).

1,4,8,11,15,18,22,25-Octaoctyltetrabenzo[b,g,l,q][5]-monoazaporphyrin (8H$_2$TBMAP). 1,4,8,11,15,18,22,25-Octaoctyltetrabenzo[*b*,*g*,*l*,*q*][5]monoazaporphinatomagnesium (40.0 mg, 0.028 mmol) in glacial acetic acid (20.0 mL) afforded the *title compound* as small fine needlelike crystals (15.0 mg, 38%). IR (cm^{-1}): ν 3295 (w, NH). MALDI-MS: isotopic cluster at *m*/*z* 1409.47 [100%, M$^+$]. Anal. Calcd for $C_{99}H_{149}N_5$: C, 84.37; H, 10.66; N, 4.97. Found: C, 84.29; H, 10.61; N, 4.92. ^{1}H NMR (400 MHz, toluene-*d*^{8}, 80 °C): δ 11.34 (s, 1H), 11.21 (s, 2H), 8.02−7.91 (m, 4H), 7.89 (s, 4H) 5.01 (t, *J* = 7.5 Hz, 8H), 4.48−4.27 (m, 8H), 2.53−2.35 (m, 16H), 1.92−1.74 (m, 16H), 1.61−1.16 (m, 80H), 0.94−0.77 (m, 24H), −0.80 (s, 2H). UV/vis (in toluene): λ = 682 nm (log ε = 5.16). Thermotropic mesophase transitions (data for the second heating and first cooling cycles): Cr 87 Col$_h$ 174 I 171 Col$_h$ 75 Cr (°C).

1,4,8,11,15,18,22,25-Octaoctyltetrabenzo[b,g,l,q]porphyrin (8H$_2$TBP). 1,4,8,11,15,18,22,25-1,4,8,11,15,18,22,25-Octaoctyltetrabenzo[*b*,*g*,*l*,*q*]porphinatomagnesium (10.0 mg, 0.007 mmol) in glacial acetic acid (20.0 mL) afforded the *title compound* as small fine needlelike crystals (2.95 mg, 30%). IR (cm^{-1}): ν 3314 (w, NH). MALDI-MS: isotopic cluster at *m*/*z* 1407.12 [100%, M$^+$]. ^{1}H NMR (400 MHz, toluene-*d*^{8}, 80 °C): δ 11.53 (s, 4H), 7.95 (s, 8H), 4.50 (t, *J* = 7.3 Hz, 16H), 2.53−2.42 (m, 16H), 1.87−1.77 (m, 16H), 1.53−1.32 (m, 48H), 1.29−1.24 (m, 16H), 0.85 (t, *J* = 7.1 Hz, 24H), −1.99 (s, 2H). UV/vis (in toluene): λ = 676 nm (log ε = 4.83). Thermotropic mesophase transitions (data for the second heating and first cooling cycles): Cr 110 Col$_h$ 179 I 174 Col$_h$ 98 Cr (°C).

General Procedure for Copper Metalation of 1,4,8,11,15,18,22,25-Octaoctyltetrabenzo[*b*,*g*,*l*,*q*](aza)-porphyrin Derivatives. In a typical experiment, the metal-free macrocycle (1 equiv) and copper acetate monohydrate (1.5 equiv) were dispersed in 1-pentanol using an ultrasonic bath. The mixture was stirred and heated at reflux for 15 min. After cooling, the product was precipitated in distilled water, extracted with DCM, and washed repeatedly with water to remove inorganic residues. The organic extract was dried with Na_2SO_4 and the solvent evaporated to give the required copper-metalated macrocycle. Column chromatography over silica gel (DCM) gave the product as a single fraction, which was recrystallized from DCM/MeOH.

1,4,8,11,15,18,22,25-Octaoctyltetrabenzo[b,g,l,q][5,10,15]-triazaporphinatocopper (8Cu^{II}TBTrAP). Following the above general procedure, 1,4,8,11,15,18,22,25-octaoctyltetrabenzo[*b*,*g*,*l*,*q*][5]-monoazaporphyrin (40.0 mg, 0.028 mmol) was reacted with copper acetate monohydrate (7.73 mg, 0.043 mmol) in 1-pentanol (10.0 mL). Column chromatography and recrystallization afforded the *title compound* as threadlike, blue-green crystals (28 mg, 67%). MALDI-MS: isotopic cluster at *m*/*z* 1470.29 [100%, M$^+$]. Anal. Calcd for $C_{97}H_{145}N_7Cu$: C, 79.10; H, 9.92; N, 6.66. Found: C, 78.97; H, 9.82; N, 6.75. UV/vis (in toluene): λ = 702 nm (log ε = 4.91). Thermotropic mesophase transitions (data for the second heating and first cooling cycles): Cr 121 Col$_r$ 156 Col$_h$ 216 I 214 Col$_h$ 154 Col$_r$ 106 Cr (°C).

1,4,8,11,15,18,22,25-Octaoctyltetrabenzo[b,g,l,q][5,10]-diazaporphinatocopper (8Cu^{II}TBcisDAP). Using the above procedure, 1,4,8,11,15,18,22,25-octaoctyltetrabenzo[*b*,*g*,*l*,*q*][5,10]diazaporphyrin (10.0 mg, 0.007 mmol) was reacted with copper acetate monohydrate (1.93 mg, 0.011 mmol) in pentanol (10.0 mL). Workup, purification, and recrystallization afforded the *title compound* as a blue solid (7.3 mg, 70%). MALDI-MS: isotopic cluster at *m*/*z* 1471.40 [100%, M$^+$]. Anal. Calcd for $C_{98}H_{146}N_6Cu$: C, 79.97; H, 10.00; N, 5.71. Found: C, 79.82; H, 9.87; N, 5.67. UV/vis (in toluene): λ = 667 nm (log ε = 5.22). Thermotropic mesophase transitions (data for the second heating and first cooling cycles): Cr 135 Col$_h$ 199 I 190 Col$_h$ 119 Cr (°C).

1,4,8,11,15,18,22,25-Octaoctyltetrabenzo[b,g,l,q][5,15]-diazaporphinatocopper (8Cu^{II}TBtransDAP). Using the above procedure, 1,4,8,11,15,18,22,25-octaoctyltetrabenzo[*b*,*g*,*l*,*q*][5,15]-diazaporphyrin (10.0 mg, 0.007 mmol) in pentanol (10.0 mL) was reacted with copper(II) acetate (7.73 mg, 0.043 mmol). Workup, purification, and recrystallization afforded the *title compound* as a blue solid (7.4 mg, 70%). MALDI-MS: isotopic cluster at *m*/*z* 1471.48 [100%, M$^+$]. Anal. Calcd for $C_{98}H_{146}N_6Cu$: C, 79.97; H, 10.00; N, 5.71. Found: C, 79.82; H, 9.77; N, 5.79. UV/vis (in toluene): λ = 698 nm (log ε = 5.23). Thermotropic mesophase transitions (data for the second heating and first cooling cycles): Cr 28 Col$_h$ 115 I 94, Col$_h$ 19 Cr (°C).

1,4,8,11,15,18,22,25-Octaoctyltetrabenzo[b,g,l,q][5]-monoazaporphinatocopper (8Cu^{II}TBMAP). Following the above procedure, 1,4,8,11,15,18,22,25-octaoctyltetrabenzo[*b*,*g*,*l*,*q*][5]-monoazaporphyrin (40.0 mg, 0.028 mmol) in pentanol (10.0 mL) was reacted with copper(II) acetate (1.93 mg, 0.011 mmol). Workup, purification, and recrystallization gave the *title compound* as a blue solid (31.4 mg, 75%). MALDI-MS: isotopic cluster at *m*/*z* 1469.62 [100%, M$^+$]. Anal. Calcd for $C_{99}H_{147}N_5Cu$: C, 80.84; H, 10.07; N, 4.76. Found: C, 80.90; H, 10.01; N, 4.70. UV/vis (in toluene): λ = 663 nm (log ε = 5.03). Thermotropic mesophase transitions (data for the second heating and first cooling cycles): Cr 62 Col$_r$ 119 Col$_h$ 196 I 189 Col$_h$ 103 Cr (°C).

1,4,8,11,15,18,22,25-Octaoctyltetrabenzo[b,g,l,q]-porphinatocopper (8Cu^{II}TBP). Using the procedure above, 1,4,8,11,15,18,22,25-octaoctyltetrabenzo[*b*,*g*,*l*,*q*]porphyrin (5.0 mg, 0.0035 mmol) in pentanol (5.0 mL) was reacted with copper(II) acetate (0.97 mg, 0.005 mmol). After workup and reprecipitation, the *title compound* was obtained as a blue amorphous solid (3.4 mg, 65%). MALDI−MS: isotopic cluster at *m*/*z* 1467.62 [100%, M$^+$]. UV/vis (in

toluene): λ = 639 nm (log ε = 4.77). Thermotropic mesophase transitions (data for the second heating and first cooling cycles): Cr 96 Col_h 237 I 223 Col_h 77 Cr (°C).

TD-DFT Calculations. Theoretical calculations were carried out using the *G03W* software package.[29] The B3LYP functional was used with 6-31G(d) basis sets for both geometry optimizations and TD-DFT calculations for the series of partial aza-substituted copper(II) complexes Cu^{II}Pc and Cu^{II}TBP. The octyl substituents were substituted with hydrogen atoms to simplify the calculations. A near-planar structure for the core of 8Cu^{II}TBTrAP has been demonstrated by X-ray crystallography in this work, vide infra. X-ray crystal structures of the 1,4,8,11,15,18,22,25-octahexyl-MgTBTrAP and -MgTBMAP complexes[10] revealed similar near-planar structures.

CONCLUSIONS

The synthetic chemistry reported in this paper confirms the findings of an earlier study from one of our laboratories that the reaction of varying equivalents of MeMgBr with 3,6-dialkylphthalonitrile provides access to mixtures of hybrid macrocycles and the TBP analogue. For the first time, both cis and trans isomers of the TBDAP macrocycle are isolated, giving access to the full series. The use of 2 or 3 equiv of MeMgBr gives the highest aggregate yield of the hybrid compounds. Chromatographic separation of the individual components of the mixtures was readily achieved, no doubt attributable to some extent to the solubility of the compounds through the presence of eight alkyl substituents at the nonperipheral positions. As expected, the new (copper) derivatives displayed columnar liquid-crystal behavior. However, it was revealed that the diazaporphyrins (8Cu^{II}TBDAPs) did not follow the general trend; the mesophase behavior for 8Cu^{II}TB*trans*DAP is particularly anomalous with both the melting and clearing points depressed by around 100 °C compared to other derivatives in the series.

Michl's perimeter model provides a readily accessible conceptual framework for analyzing and predicting trends observed in the experimental and calculated optical spectra. The trends in the spectra and DFT calculations for the 8Cu^{II}TBMAP, 8Cu^{II}TB*trans*DAP, 8Cu^{II}TBcisDAP, and 8Cu^{II}TBTrAP complexes were found to be fully consistent with those reported previously for the dianion species of TBMAP, TB*cis*DAP, TB*trans*DAP, and TBTrAP on the basis of semiempirical ZINDO calculations.[16]

AUTHOR INFORMATION

Corresponding Author

*E-mail: a.cammidge@uea.ac.uk (A.N.C.), m.cook@uea.ac.uk (M.J.C.), nagaok@m.tohoku.ac.jp (N.K.). Tel: +44 (0)1603-592011 (A.N.C.), +44 (0)1603-593135 (M.J.C.), +81 (0)22-795-7719 (N.K.). Fax: +44 (0)1603-592011 (A.N.C.), +44 (0)1603-592003 (M.J.C.), +81 (0)22-795-7719 (N.K.).

Present Address

[†]Department of Chemistry, Rhodes University, 6140 Grahamstown, South Africa.

Notes

The authors declare no competing financial interest.

ACKNOWLEDGMENTS

This work was supported by a Grant-in-Aid for Scientific Research from the Ministry of Education, Culture, Sports, Science and Technology, Japan [Grant 20108007 (π space) to N.K.]. The University of East Anglia group thanks CONACYT (Mexico) for financial support to L.S.-V. M.J.C. gratefully acknowledges the award of a Leverhulme Emeritus Fellowship from the Leverhulme Foundation. S.J.C. and G.J.T. thank the EPSRC for funding.

REFERENCES

(1) Kobayashi, N. In *The Porphyrin Handbook*; Kadish, K. M., Smith, K. M., Guilard, R., Eds.; Academic Press: New York, 2003; Vol. *15*, pp 161−262.

(2) Cammidge, A. N.; Chambrier, I.; Cook, M. J.; Sosa-Vargas, L. In *Handbook of Porphyrin Science: With Applications to Chemistry, Physics, Materials Science, Engineering, Biology and Medicine*; Kadish, K. M., Smith, K. M., Guilard, R., Eds.; World Scientific: Singapore, 2012; Vol. *16*, pp 331−404.

(3) (a) Helberger, J. H.; von Rebay, A. *Justus Liebigs Ann. Chem.* **1937**, *531*, 279−287. (b) Helberger, J. H. *Justus Liebigs Ann. Chem.* **1937**, *529*, 205−218.

(4) Dent, C. E. *J. Chem. Soc.* **1938**, 1−6.

(5) (a) Barrett, P. A.; Linstead, R. P.; Tuey, G. A. P.; Robertson, J. M. *J. Chem. Soc.* **1939**, 1809−1820. (b) Barrett, P. A.; Linstead, R. P.; Rundall, F. G.; Tuey, G. A. P. *J. Chem. Soc.* **1940**, 1079−1092.

(6) (a) Yakubov, L. A.; Galanin, N. E.; Shaposhnikov, G. P. *Russ. J. Org. Chem.* **2008**, *44*, 755−760. (b) Galanin, N. E.; Kudrik, E. V.; Shaposhnikov, G. P. *Russ. J. Gen. Chem.* **2004**, *74*, 282−285. (c) Galanin, N. E.; Kudrik, E. V.; Shaposhnikov, G. P. *Russ. J. Gen. Chem.* **2005**, *75*, 651−655. (d) Galanin, N. E.; Kudrik, E. V.; Shaposhnikov, G. P. *Russ. J. Org. Chem.* **2002**, *38*, 1200−1203. (e) Galanin, N. E.; Yakubov, L. A.; Kudrik, E. V.; Shaposhnikov, G. P. *Russ. J. Gen. Chem.* **2008**, *78*, 1436−1440. (f) Galanin, N. E.; Shaposhnikov, G. P. *Russ. J. Gen. Chem.* **2007**, *77*, 1951−1954.

(7) (a) Leznoff, C. C.; McKeown, N. B. *J. Org. Chem.* **1990**, *55*, 2186−2190. (b) Tse, Y.-H.; Goel, A.; Hu, M.; Lever, A. B. P.; Leznoff, C. C.; Van Lier, J. E. *Can. J. Chem.* **1993**, *71*, 742−753.

(8) Makarova, E. A.; Kopranenkov, V. N.; Shevtsov, V. K.; Lukyanets., E. A. *Chem. Heterocycl. Compd.* **1989**, *25*, 1159−1164.

(9) (a) Khelevina, O. G.; Berezin, B. D.; Petrov, O. A.; Glazunov, A. V. *Koord. Khim.* **1990**, *16*, 1047−1052. (b) Ivanova, Y. B.; Churakhina, Y. I.; Semeikin, A. S.; Mamardashvili, N. Z. *Russ. J. Gen. Chem.* **2009**, *79*, 833−838. (c) Cammidge, A. N.; Cook, M. J.; Hughes, D. L.; Neckelson, F.; Rahman, M. *Chem. Commun.* **2005**, 930−932.

(10) Cammidge, A. N.; Chambrier, I.; Cook, M. J.; Hughes, D. L.; Rahman, M.; Sosa-Vargas, L. *Chem.—Eur. J.* **2011**, *17*, 3136−3146.

(11) (a) Michl, J. *J. Am. Chem. Soc.* **1978**, *100*, 6801−6811. (b) Michl, J. *Tetrahedron* **1984**, *40*, 3845−3934.

(12) McKeown, N. B.; Chambrier, I.; Cook, M. J. *J. Chem Soc., Perkin Trans. 1* **1990**, 1169−1177.

(13) Cherodian, A. S.; Davies, A. N.; Richardson, R. M.; Cook, M. J.; McKeown, N. B.; Thomson, A. J.; Feijo, J.; Ungar, G.; Harrison, K. J. *Mol. Cryst. Liq. Cryst.* **1991**, *196*, 103−114.

(14) Cammidge, A. N.; Chambrier, I.; Cook, M. J.; Langner, E. H. G.; Rahman., M.; Swarts, J. C. *J. Porphyrins Phthalocyanines* **2011**, *15*, 890−897.

(15) Mack, J.; Stillman, M. J.; Kobayashi, N. *Coord. Chem. Rev.* **2007**, *251*, 429−453.

(16) Mack, J.; Kobayashi, N.; Leznoff, C. C.; Stillman, M. J. *Inorg. Chem.* **1997**, *36*, 5624−5634.

(17) (a) Seth, M.; Ziegler, T.; Banerjee, A.; Autschbach, J.; van Gisbergen, S. J. A.; Baerends, E. J. *J. Chem. Phys.* **2004**, *120*, 10942−10954. (b) Seth, M.; Autschbach, J.; Ziegler, T. *J. Chem. Phys.* **2005**, *122*, 094112. (c) Seth, M.; Ziegler, T. *J. Chem. Phys.* **2006**, *124*, 144105. (d) Seth, M.; Autschbach, J.; Ziegler, T. *J. Chem. Theory Comput.* **2007**, *3*, 434−447. (e) Krykunov, M.; Seth, M.; Ziegler, T.; Autschbach, J. *J. Chem. Phys.* **2007**, *127*, 244102. (f) Seth, M.; Krykunov, M.; Ziegler, T.; Autschbach, J.; Banerjee, A. *J. Chem. Phys.* **2008**, *128*, 144105. (g) Seth, M.; Krykunov, M.; Ziegler, T.; Autschbach, J. *J. Chem. Phys.* **2008**, *128*, 2341025. (h) Seth, M.; Ziegler, T.; Autschbach, J. *J. Chem. Phys.* **2008**, *129*, 104105. (i) Peralta, G. A.; Seth, M.; Ziegler, T. *Inorg. Chem.* **2007**, *46*, 9111−9125.

(18) Gouterman, M. In *The Porphyrins*; Dolphin, D., Ed.; Academic Press: New York, 1978; Vol. *3*, pp 1−165.
(19) (a) Moffitt, W. J. *J. Chem. Phys.* **1954**, *22*, 320−333. (b) Moffitt, W. J. *J. Chem. Phys.* **1954**, *22*, 1820−1829.
(20) Mack, J.; Stillman, M. J. In *The Porphyrin Handbook*; Kadish, K. M., Smith, K. M., Guilard, R., Eds.; Academic Press: New York, 2003; Vol. *16*, pp 43−116.
(21) Mack, J.; Stillman, M. J. *Coord. Chem. Rev.* **2001**, *219−221*, 993−1032.
(22) Perrin, M. H. *J. Chem. Phys.* **1973**, *59*, 2090−2104.
(23) Kobayashi, N. Konami, H. In *Phthalocyanine. Principles and Properties*; Leznoff, C. C., Lever, A. B. P., Eds.; VCH Publications: New York, 1996; Vol. *4*, pp 343−404.
(24) Ogata, H.; Fukuda, T.; Nakai, K.; Fujimura, Y.; Neya, S.; Stuzhin, P. A.; Kobayashi, N. *Eur. J. Inorg. Chem.* **2004**, 1621−1629.
(25) Mack, J.; Asano, Y.; Kobayashi, N.; Stillman, M. J. *J. Am. Chem. Soc.* **2005**, *127*, 17697−17711.
(26) (a) Stillman, M. J.; Nyokong, T. In *Phthalocyanine. Principles and Properties*; Leznoff, C. C., Lever, A. B. P., Eds.; VCH Publications: New York, 1989; Vol. *1*, pp 133−289. (b) Stillman, M. J. In *Phthalocyanine. Principles and Properties*; Leznoff, C. C., Lever, A. B. P., Eds.; VCH Publications: New York, 1993; Vol. *3*, pp 227−296. (c) Mack, J.; Stillman, M. J. *Coord. Chem. Rev.* **2001**, *219−221*, 993−1032.
(27) Piepho, S. B.; Schatz, P. N. In *Group Theory in Spectroscopy with Applications to Magnetic Circular Dichroism*; Wiley: New York, 1983.
(28) Coles, S. J.; Gale, P. A. *Chem. Sci.* **2012**, *30*, 683−689.
(29) Frisch, M. J.; Trucks, G. W.; Schlegel, H. B.; Scuseria, G. E.; Robb, M. A.; Cheeseman, J. R.; Montgomery, J. A., Jr.; Vreven, T.; Kudin, K. N.; Burant, J. C.; Millam, J. M.; Iyengar, S. S.; Tomasi, J.; Barone, V.; Mennucci, B.; Cossi, M.; Scalmani, G.; Rega, N.; Petersson, G. A.; Nakatsuji, H.; Hada, M.; Ehara, M.; Toyota, K.; Fukuda, R.; Hasegawa, J.; Ishida, M.; Nakajima, T.; Honda, Y.; Kitao, O.; Nakai, H.; Klene, M.; Li, X.; Knox, J. E.; Hratchian, H. P.; Cross, J. B.; Bakken, V.; Adamo, C.; Jaramillo, J.; Gomperts, R.; Stratmann, R. E.; Yazyev, O.; Austin, A. J.; Cammi, R.; Pomelli, C.; Ochterski, J. W.; Ayala, P. Y.; Morokuma, K.; Voth, G. A.; Salvador, P.; Dannenberg, J. J.; Zakrzewski, V. G.; Dapprich, S.; Daniels, A. D.; Strain, M. C.; Farkas, O.; Malick, D. K.; Rabuck, A. D.; Raghavachari, K.; Foresman, J. B.; Ortiz, J. V.; Cui, Q.; Baboul, A. G.; Clifford, S.; Cioslowski, J.; Stefanov, B. B.; Liu, G.; Liashenko, A.; Piskorz, P.; Komaromi, I.; Martin, R. L.; Fox, D. J.; Keith, T.; Al-Laham, M. A.; Peng, C. Y.; Nanayakkara, A.; Challacombe, M.; Gill, P. M. W.; Johnson, B.; Chen, W.; Wong, M. W.; Gonzalez, C.; Pople, J. A. *Gaussian 03*, revision C.02; Gaussian, Inc.: Wallingford, CT, 2004.